

RESEARCH PAPER



## TNFAIP8L2/TIPE2 impairs autolysosome reformation via modulating the RAC1-MTORC1 axis

Wen Li<sup>a</sup>, Yulan Li<sup>a</sup>, Yetong Guan<sup>ib</sup>, Yingxin Du<sup>a</sup>, Mingsheng Zhao<sup>a</sup>, Xiaotong Chen<sup>a</sup>, Faliang Zhu<sup>a</sup>, Chun Guo<sup>a</sup>, Yufeng Jia<sup>a</sup>, Yuan Li<sup>a</sup>, Xiaoyu Wang<sup>a</sup>, Xiaoyan Wang<sup>a</sup>, Yongyu Shi<sup>a</sup>, Qun Wang<sup>a</sup>, Yan Li<sup>b</sup>, and Lining Zhang<sup>a</sup>

<sup>a</sup>Department of Immunology, School of Basic Medical Science, Shandong University, Jinan, China; <sup>b</sup>Department of Pathogen Biology, School of Basic Medical Science, Shandong University, Jinan, China

### ABSTRACT

Macroautophagy/autophagy is an evolutionarily conserved process that involves the selective degradation of cytoplasmic components within lysosomes in response to starvation. Autophagy is an ancient defense mechanism that has been closely integrated with the immune system and has multiple effects on innate and adaptive immunity. The pro-inflammatory and anti-inflammatory cytokines can activate and inhibit autophagy, respectively. TNFAIP8L2/TIPE2 (tumor necrosis factor, alpha-induced protein 8-like 2) is a newly identified immune negative regulator of innate and adaptive immunity that plays an important role in immune homeostasis. However, whether and how TNFAIP8L2 controls autophagy is still unknown. Murine TNFAIP8L2 can directly bind to and block the RAC1 GTPase activity to regulate innate immunity. RAC1 can also bind to MTOR and regulate MTORC1 cellular localization and activity. Here, we find that TNFAIP8L2 can compete with MTOR for binding to the GTP-bound state of RAC1 and negatively regulate MTORC1 activity. Interestingly, TNFAIP8L2 overexpression fails to induce autophagy flux by the suppression of the MTOR activity under glutamine and serum starvation. Instead, TNFAIP8L2 appears to impair autophagic lysosome reformation (ALR) during prolonged starvation. Finally, we demonstrate that TNFAIP8L2 overexpression leads to a defect in MTOR reactivation and disrupts autophagy flux, thereby leading to cell death. Furthermore, TNFAIP8L2 deficiency can exacerbate the inflammatory response and lung injury by controlling the MTOR activity in an LPS-induced mouse endotoxemia model. Our study reveals a novel role of TNFAIP8L2 in autophagy by regulating the RAC1-MTORC1 axis that supports its potential as a target for therapeutic treatment.

**Abbreviations:** ALR: autophagic lysosome reformation; BafA<sub>1</sub>: bafilomycin A<sub>1</sub>; BMDMs: bone marrow-derived macrophages; Co-IP: Co-Immunoprecipitation; LAMP1: lysosomal associated membrane protein 1; MAP1LC3B/LC3B: microtubule associated protein 1 light chain 3 beta; MTORC1: mechanistic target of rapamycin kinase complex 1; RAPA: rapamycin; RPS6: ribosomal protein S6; SQSTM1/p62: sequestosome 1; Starv: Starvation; TNFAIP8L2/TIPE2: tumor necrosis factor-alpha-induced protein-8 like-2.

### ARTICLE HISTORY

Received 15 August 2019  
Revised 21 April 2020  
Accepted 23 April 2020

### KEYWORDS





Autophagy; autophagic lysosome reformation (ALR); cell death; MTORC1; RAC1; TNFAIP8L2/TIPE2


### Introduction

Autophagy influences immunity and inflammation, while immune signaling, in turn, regulates autophagy [1,2]. Pro-inflammatory cytokines, such as IFNG, activate autophagy, whereas anti-inflammatory cytokines, such as IL4 and IL13, inhibit autophagy [3,4]. TNFAIP8L2/TIPE2 (tumor necrosis factor, alpha-induced protein-8 like-2) is a recently identified negative regulator of innate and adaptive immunity that plays an important role in immune homeostasis [5–8]. *Tnfaip8l2* deficiency in mice leads to multiple organ inflammation, and *TNFAIP8L2* downregulation in humans is associated with systemic autoimmunity [5,9]. Moreover, TNFAIP8L2 is a biomarker and inhibitor of tumor progression by targeting the RAS signaling pathway [10]. Recently, TNFAIP8L2 has been evidenced to bind phosphoinositide species, such as phosphatidylinositol 4,5-bisphosphate (PtdIns [4,5]P<sub>2</sub>) and

phosphatidylinositol 3,4,5-trisphosphate (PtdIns [3–5]P<sub>3</sub>) to promote leukocyte leading-edge formation and polarity [11]. Our previous research supports the idea that the well-characterized signal-transducing molecule RAC1 (amino acids 1–192), a Rho-family GTPase, is a target for TNFAIP8L2 to suppress angiogenesis and non-small cell lung cancer (NSC-23766LC) invasiveness [12,13]. It should be mentioned that TNFAIP8L2 can directly bind to the RAC1 C-terminal CAAX motif and block its GTPase activity to control infections and innate immunity through Toll-like receptors (TLR) [14]. However, the role of TNFAIP8L2 in autophagy has not been described.

MTOR, a serine/threonine kinase, comprises of two separate complexes, MTORC1 and MTORC2, which exhibit specificity for different sets of effectors, and simultaneously senses energy, nutrients, stress, and growth factors to control cell growth and division [15,16]. MTORC1 signaling is

**CONTACT** Yan Li  [liyan2015@sdu.edu.cn](mailto:liyan2015@sdu.edu.cn)  Department of Pathogen Biology, School of Basic Medical Science, Shandong University, Jinan, China; Lining Zhang  [zhanglining@sdu.edu.cn](mailto:zhanglining@sdu.edu.cn)  Department of Immunology, School of Basic Medical Science, Shandong University, 44# Wenhua Xi Road, Jinan 250012, China

 Supplemental data for this article can be accessed [here](#).

conventionally stimulated by amino acids and growth factors stimulation. In response to the amino acid signal, MTORC1 is recruited to the lysosomal surface through active RAG GTPases and Ragulator, a pentameric protein complex that anchors the RAG GTPases to the lysosomes [17–19]. Upon MTORC1 translocation to the lysosomal membrane, MTORC1 is then activated by the guanosine-5'-triphosphate (GTP)-binding of the small GTPase RHEB in the presence of growth factors [15,20,21]. Therefore, both amino acid-dependent MTORC1 lysosomal localization and MTORC1 activation, by active RHEB in response to growth factors, are essential and required for MTORC1 signaling. Interestingly, RAC1 is also able to bind directly to MTOR through its C-terminal domain, thereby altering MTORC1 and MTORC2 localization at certain membranes and regulating their activation [22]. However, the ability of RAC1 to translocate to the lysosome membrane and its correlation with the GTPase activity has not been evaluated yet. Additionally, how RAC1 relates to the RAG GTPases and RHEB regarding the control of MTOR also requires further investigation.

Upon nutrient deficiency, MTOR is inactivated and, therefore, can no longer repress autophagy. Autophagy is a universally conserved, self-digestive process in which cytoplasmic protein aggregates and damaged organelles are translocated to the lysosomes for degradation [23–26]. This process has been shown to play critical roles in many physiological and pathological conditions [27–29]. Autophagy includes several sequential stages: intracellular components sequestration by autophagosome, autolysosome formation by fusion of the autophagosome with the lysosome, degradation of the enclosed contents by lysosomal hydrolases, autophagy termination, and autolysosomes reformation (ALR) [30,31]. Autophagy initiation requires MTOR inhibition, whereas MTOR reactivation is necessary for ALR to attenuate autophagy and restore mature lysosomes during prolonged starvation [30–32].

Since the C-terminal domain of RAC1 can directly bind both MTOR and TNFAIP8L2, we hypothesized that TNFAIP8L2 might influence MTOR activity via RAC1 to affect autophagy flux. In this study, we proposed that TNFAIP8L2 negatively controls MTORC1 activity through RAC1 and impairs ALR in glutamine- and serum starvation-induced autophagy. By targeting MTORC1, TNFAIP8L2 exhibited anti-inflammation effects in an LPS-induced mouse model of inflammation. Therefore, TNFAIP8L2 may be a therapeutic target for autophagy- and inflammation-related diseases.

## Results

### **TNFAIP8L2 impairs autophagy flux following starvation and induces cell death**

To address the role of TNFAIP8L2 in autophagy, we first overexpressed TNFAIP8L2 exogenously and assessed the autophagy activity in the HepG2 cell line, in which endogenous TNFAIP8L2 was not expressed (Figure S1). We found that overexpressing TNFAIP8L2 increased both the levels of

LC3B-II and the autophagy degradation substrate, SQSTM1/p62, in normal growth condition (Figure 1A). Upon starvation, however, autophagy can no longer be repressed, and the level of SQSTM1 was gradually reduced in wild type cells as previously observed (Figure 1A) [33–35]. Although TNFAIP8L2 overexpression led to higher levels of LC3B-II compared to wild type, it caused more accumulation of SQSTM1, suggesting that autophagy flux was impaired (Figure 1A).

To further confirm effect of TNFAIP8L2 on autophagy, we generated BMDMs from WT and *tnfaip8l2* knockout mice. The genotype of the *tnfaip8l2*<sup>-/-</sup> mice was confirmed by PCR, and the phenotype of *Tnfaip8l2* deficiency in BMDMs was confirmed by mRNA detection (Figure S2A and S2B). In *Tnfaip8l2*-deficient BMDMs, both LC3B-II and SQSTM1 levels showed significant decreases in the normal growth condition (Figure 1B). Further, the SQSTM1 degradation rate was enhanced under starvation for 2 h, implying that TNFAIP8L2 deficiency promoted autophagy flux (Figure 1B). Next, we used the autophagy flux reporter mCherry-EGFP-LC3 to monitor the dynamics of autophagy flux. When autophagy is active, autolysosomes enclose LC3B, and the EGFP signal would disappear in response to the low lysosomal pH [36]. Therefore, the increase of autolysosome indicated by the mCherry signal demonstrates that autophagy flux is activated [37,38]. As shown in Figure 1C, TNFAIP8L2 obviously decreased the transition of mCherry<sup>+</sup> EGFP<sup>+</sup> autophagosomes (yellow puncta) to mCherry<sup>+</sup> EGFP<sup>-</sup> autolysosomes (red puncta) compared to control cells under starvation for 1 h. Moreover, the total number of LC3 puncta (yellow and red) in TNFAIP8L2-overexpressing cells was about 2.5- and 1.5-fold higher than control cells under normal and starvation conditions, respectively (Figure 1C), implying interference with autophagy flux.

We further examined which stage would likely be controlled by TNFAIP8L2. We, therefore, measured the changes in LC3B and SQSTM1 in response to the MTOR inhibitor, rapamycin and inhibitor of the autophagosome-lysosome fusion, bafilomycin A<sub>1</sub>, separately. As shown in Figure 2A and C, the treatment with bafilomycin A<sub>1</sub> had no obvious impact on the differences of LC3B-II and SQSTM1 induced by TNFAIP8L2; however, rapamycin treatments almost completely abolished these differences in both HepG2 and BMDMs cell lines. Further, the immunofluorescence analysis results were consistent with these previous findings (Figure 2B and D). These data suggest that TNFAIP8L2 impairs the autophagy-dependent MTOR activity, rather than influencing autophagosome-lysosome fusion.

Since autophagy initiation requires MTOR inhibition and ALR needs MTOR reactivation, we next explored how TNFAIP8L2 regulates these two processes. When TNFAIP8L2 was overproduced, the numbers of autolysosomes indicated by LAMP1<sup>+</sup>LC3B<sup>+</sup> (yellow) puncta were significantly decreased after 4 h of starvation, and its mean size was clearly much larger than wild type cells after 0 h, 8 h, and 10 h of starvation (Figure 2E). Further, much fewer lysosomes (LAMP<sup>+</sup> vesicles) were regenerated in TNFAIP8L2-overexpressing cells after prolonged starvation for 8 h and 10 h (Figure 2E). These data showed that ALR was impaired,

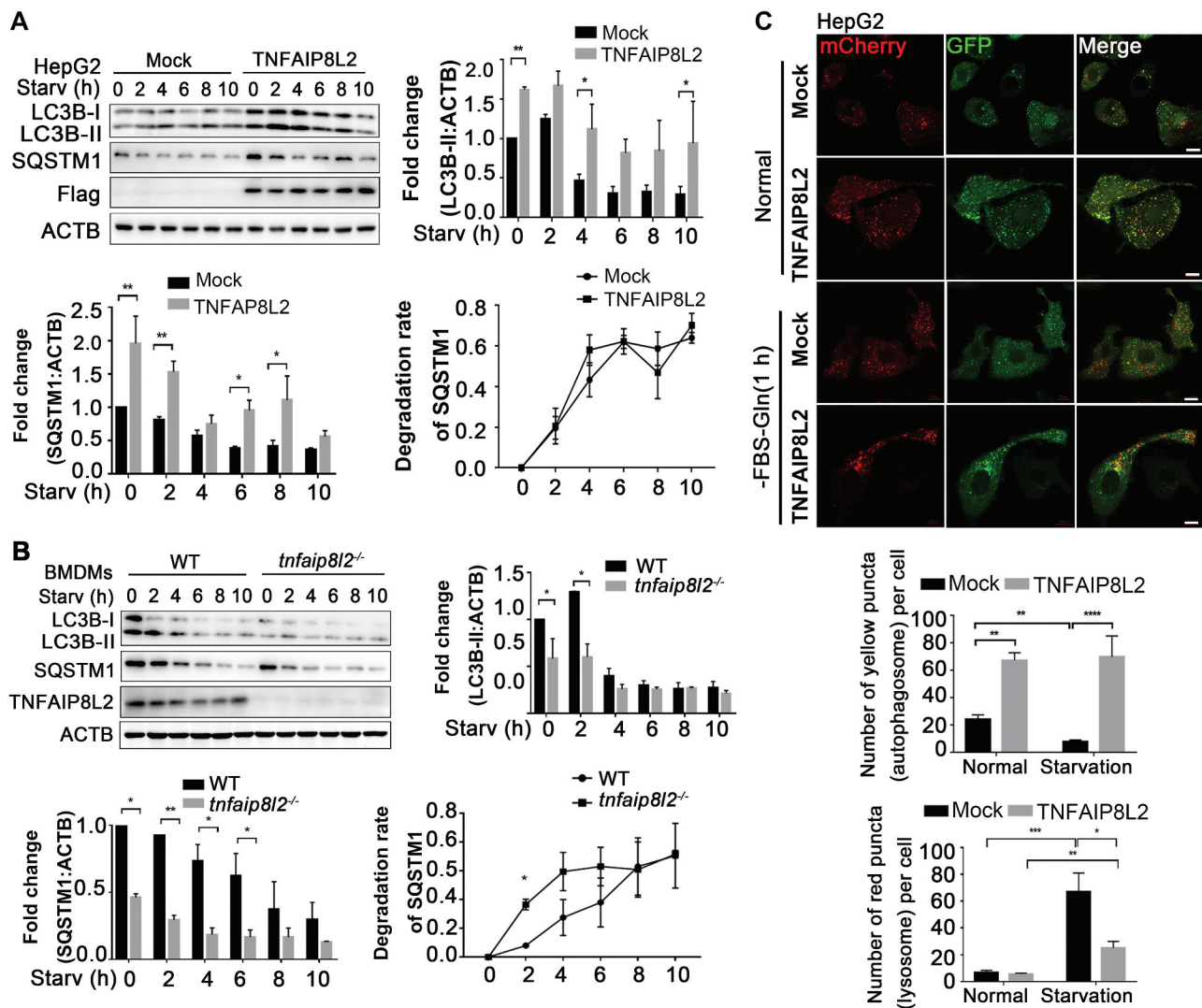


**Figure 1.** TNFAIP8L2 impairs autophagy flux. HepG2 cells transfected with the empty vector or *Flag-TNFAIP8L2* plasmid (A) and BMDMs from WT or *Tnfaip8l2*-deficient mice (B) were starved for 0, 2, 4, 6, 8, and 10 h. Cell lysates were analyzed by immunoblotting using the indicated antibodies. Quantitative analyses of LC3B-II and SQSTM1 and degradation ratio of SQSTM1 were performed by Photoshop software. Values are mean  $\pm$  SEM ( $n = 3$ ). (C) The *mCherry-EGFP-Lc3b* adenovirus was transfected to HepG2 cells with or without TNFAIP8L2, and cells were starved for 1 h. Scale bars: 10  $\mu$ m. The signals of *mCherry*<sup>+</sup> *EGFP*<sup>+</sup> (yellow) and *mCherry*<sup>+</sup> *EGFP*<sup>-</sup> (red) signal were quantified and statistical results were presented as mean  $\pm$  SEM ( $n \geq 10$ ). Average value in vector-transfected cells without any treatment was normalized to 1 in the western blotting quantitative calculations. Statistical analysis was performed using two-way ANOVA in (A-H): \* $p < 0.05$ , \*\* $p < 0.01$ , \*\*\* $p < 0.001$ , \*\*\*\* $p < 0.0001$ .

and the full complement of lysosomes restoration was blocked. Consequently, the induction of cell death by TNFAIP8L2 was further observed as a result of impaired autophagy (Figure 2F). Altogether, we conclude that TNFAIP8L2 can inhibit ALR and impair autophagy flux to subsequently induce cell death.

### TNFAIP8L2 inhibits autolysosome reformation via negatively modulating MTOR reactivation

MTOR reactivation by the degradation of autolysosomal products is essential and required for ALR with prolonged starvation by facilitating lysosomal homeostasis and guaranteeing autophagy flux [30–32]. Since TNFAIP8L2 can affect lysosome restoration during prolonged starvation, we hypothesized that TNFAIP8L2 could also inhibit MTOR reactivation following prolonged starvation. In the cell line

HepG2, we found that TNFAIP8L2 overexpression indeed inhibited MTORC1 reactivation after 8 h and 10 h of starvation, as indicated by western blotting of the phosphorylation of both MTOR and RPS6/S6 (Ser235/236), a substrate of the MTOR pathway (Figure 3A). We also observed the TNFAIP8L2-mediated inhibition of MTOR reactivation in the H1975 cell line after starvation (Figure S3). Moreover, the p-RPS6 level appeared to be much lower in both normal and starvation conditions after 10 h of TNFAIP8L2 overexpression (Figure 3B). In contrast, *Tnfaip8l2* deletion significantly enhanced MTOR reactivation after 6 h of starvation (Figure 3C). Using immunofluorescence analysis, MTOR reactivation was also increased by the *Tnfaip8l2* deficiency under 4 h of starvation (Figure 3D). Together, this data clearly indicated that TNFAIP8L2 could suppress MTOR reactivation in the ALR process during prolonged starvation-induced autophagy.

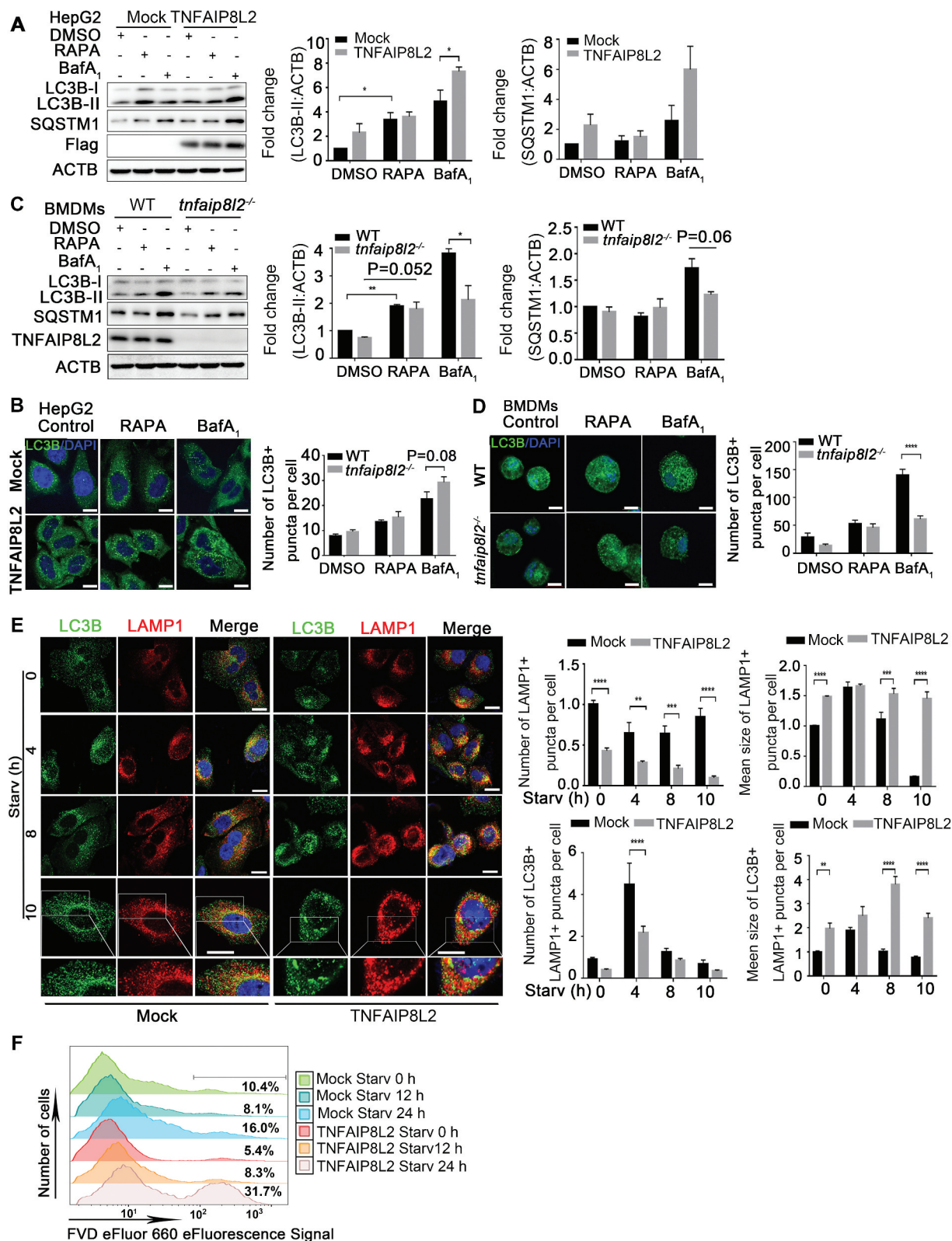


**Figure 2.** TNFAIP8L2 impairs autophagic lysosome reformation and contributes to cell death. (A) HepG2 cells were transfected with the empty vector or *Flag-TNFAIP8L2* plasmid for 24 h and then treated with rapamycin (RAPA, 5  $\mu$ M) or BafA<sub>1</sub> (10 nM) for 6 h. (B) Confocal microscopy images of LC3B were obtained from HepG2 cells treated as in (A). BMDMs were treated as in (A) and performed western blotting (C) and immunofluorescence (D). The levels of LC3B and SQSTM1 were determined by western blotting and quantified with statistical analysis. Values are mean  $\pm$  SEM (n = 3). Scale bar: 10  $\mu$ m. LC3B-positive dots (green) were quantified by Image Pro Plus software (IPP). (E) HepG2 cells with or without overexpressing Flag- TNFAIP8L2 were fixed and immunostained for LC3B and LAMP1 after starvation for 0, 4, 8, and 10 h. Scale bars: 10  $\mu$ m. Quantitative calculations of both LAMP1- and LC3B-positive puncta (number and size) and LAMP1-positive puncta (number and size) were performed by Image Pro Plus software (IPP). Values are mean  $\pm$  SEM (n  $\geq$  20). (F) HepG2 cells transfected with empty vector or *Flag-TNFAIP8L2* plasmids were induced death by starvation for 0, 12, and 24 h. Cell death was analyzed by flow cytometry. Average value in vector-transfected cells without any treatment was normalized to 1 in the quantitative calculations, including western blotting and immunofluorescence. Statistical analysis was performed using two-way ANOVA in (A-E): \*p < 0.05, \*\*p < 0.01, \*\*\*p < 0.001, \*\*\*\*p < 0.0001.

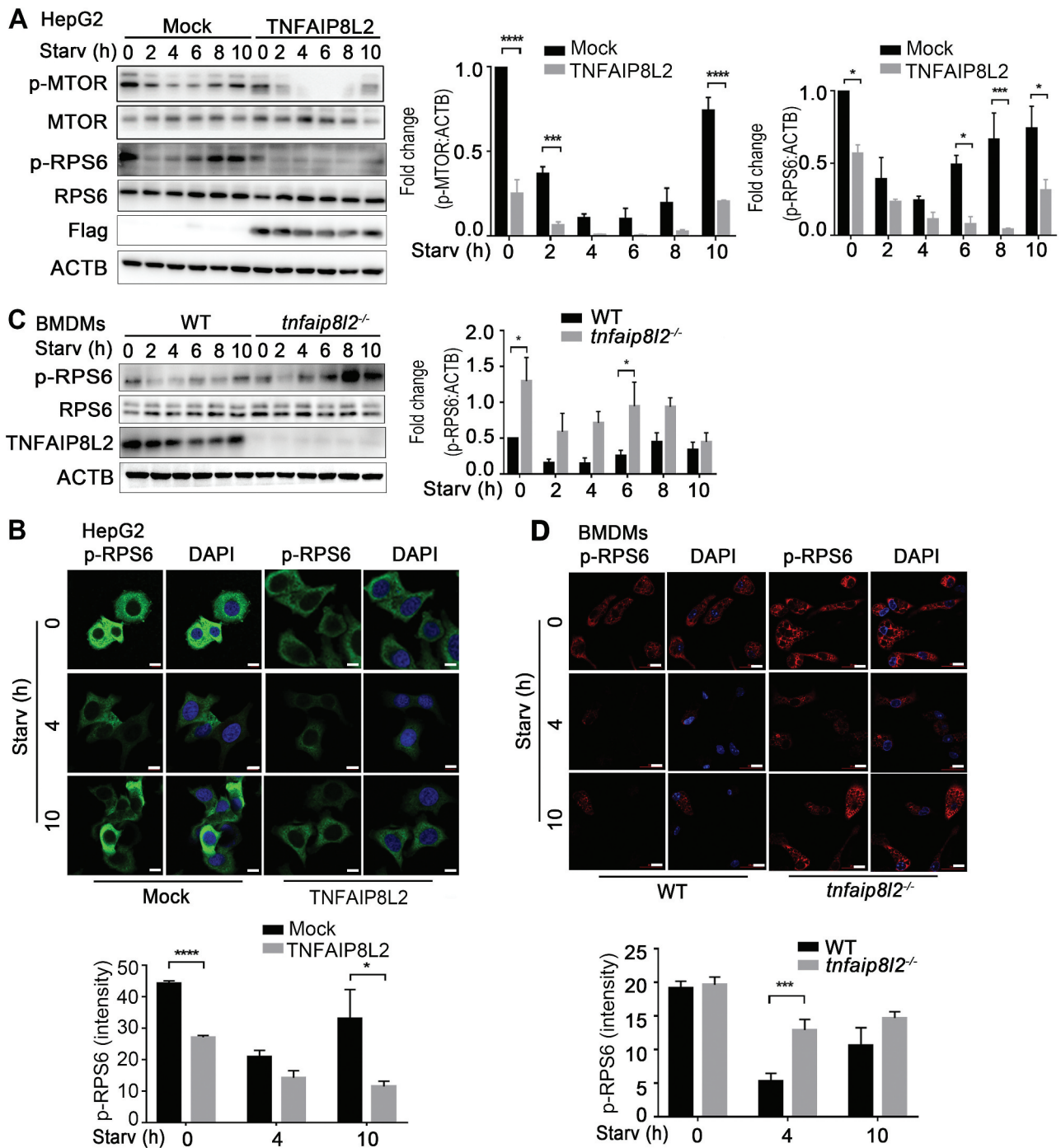


**Figure 3.** TNFAIP8L2 inhibits MTOR activation and reactivation during long starvation. HepG2 cells transfected with empty vector and *Flag-TNFAIP8L2* plasmids for 24 h (A) and BMDMs from *Tnfaip8l2*-deficient mice (C) were starved for 0, 2, 4, 6, 8 and 10 h. The phosphorylation and total level of MTOR and RPS6 were evaluated by western blotting. The quantitative analysis of p-MTOR and p-RPS6 signals was performed by Photoshop software. Values are mean  $\pm$  SEM ( $n = 3$ ). Average value in vector-transfected cells or WT BMDMs without any treatment was normalized to 1. HepG2 cells with or without overexpressing TNFAIP8L2 (B) and BMDMs (D) were starved for 0, 4, and 10 h. Then cells were stained with anti-p-RPS6 and DAPI and analyzed by confocal microscopy. The quantitative analysis of p-RPS6 intensity was performed by Zeiss Automeasure software. Scale bars: 20  $\mu$ m. Values are mean  $\pm$  SEM ( $n \geq 20$ ). Statistical analysis was performed using two-way ANOVA in (A, B) and Student's *t*-test analysis in (C, D). \* $p < 0.05$ , \*\* $p < 0.01$ , \*\*\* $p < 0.001$ .

### **TNFAIP8L2 interacts with RAC1 and enables the dissociation of the RAC1-MTOR complex**

We sought to explore whether TNFAIP8L2 controls MTOR activity by directly binding to either MTOR or RAC1. To test this hypothesis, we conducted co-immunoprecipitation (Co-IP) experiments to examine the interactions of TNFAIP8L2,

MTOR, and RAC1. First, we confirmed that RAC1 could bind to MTOR in HEK-293 T cells (Figure 4A). Next, we expressed *Flag-TNFAIP8L2* in HEK-293 T cells, and the interaction of TNFAIP8L2 with RAC1 or MTOR was evaluated by co-IP assays. Then, we found that TNFAIP8L2 was physically associated with RAC1 rather than MTOR (Figure 4B).

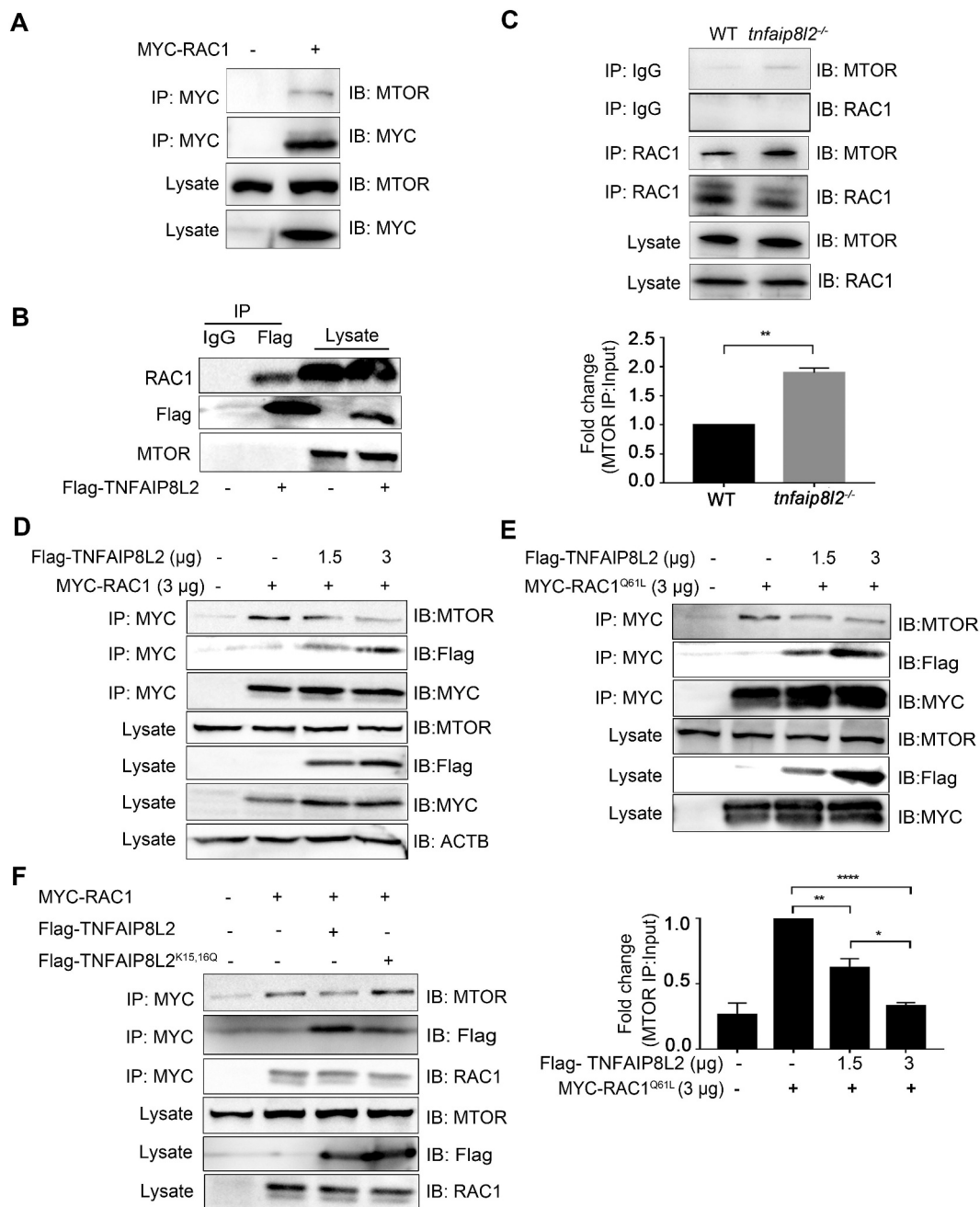


**Figure 4.** TNFAIP82 interacts with RAC1 and interrupts the interactions between RAC1 and MTOR. (A) Total cell lysates of HEK-293 T cells were incubated with anti-MYC antibody, and immunoprecipitates were subjected to western blotting with anti-MTOR and anti-MYC antibody. (B) HEK-293 T cells were transfected with the empty vector or *Flag-TNFAIP82* plasmids for 24 h, and the cell lysates were subjected to immunoprecipitation with anti-Flag, followed by anti-Flag, anti-RAC1, and anti-MTOR detection with western blotting. (C) Total cell lysates of BMDMs from WT or *Tnfaip82*-deficient mice were immunoprecipitated with anti-RAC1 antibody or anti-mouse IgG, and then blotted with anti-MTOR and anti-TNFAIP82 antibodies individually. The quantitative analysis of MTOR was performed by Photoshop software. WT BMDMs were normalized to 1. Values are mean  $\pm$  SEM (n = 2). HEK-293 T cells were transfected with WT MYC-RAC1 (D) and MYC-RAC1<sup>Q61L</sup> (E) in the presence of increasing *Flag-TNFAIP82* plasmids (0, 1.5, and 3 μg). Cells were lysed and immunoprecipitated with anti-MYC antibody. The resulting precipitates were incubated with anti-Flag, anti-MTOR, and anti-RAC1 antibodies, respectively. (F) HEK-293 T cells were transfected with MYC-RAC1 and WT *Flag-TNFAIP82* or *Flag-TNFAIP82*<sup>K15,16Q</sup> mutant plasmid, as indicated. The immunoprecipitations were performed with anti-MYC antibody, and then the precipitates were analyzed by immunoblotting with anti-Flag, anti-MTOR, and anti-RAC1 antibodies, separately. Band intensity quantifications of MTOR (C, E) were performed by Photoshop software. Values are mean  $\pm$  SEM (n = 3). Statistical analysis was performed using Student's t-test analysis in (C, E): \*p < 0.05, \*\*p < 0.01, \*\*\*\*p < 0.0001.

Previous reports demonstrate that the amino acids 185–187 (arginine, lysine, and arginine, RKR) of RAC1 in the C-terminal domain are crucial for its binding to MTOR, while the CAAX domain (amino acids 189–192) mediates its interaction with TNFAIP82. Only one amino acid is left (amino acid 188) between these two domains [14,22]. We, then, hypothesized that TNFAIP82 might compete with

MTOR for RAC1 binding. To test this hypothesis, we found that much more RAC1 was bound to MTOR in the absence of TNFAIP82 (Figure 4C). When we overexpressed MYC-RAC1 with increasing amounts of *Flag-TNFAIP82* in HEK-293 T cells, we observed that the amount of MTOR binding to RAC1 gradually decreased in response to increasing TNFAIP82 (Figure 4D).

To further examine whether TNFAIP8L2 influences the interaction of active RAC1 with MTOR, we overexpressed MYC-RAC1<sup>Q61 L</sup> with increasing amounts of TNFAIP8L2 in HEK-293 T cells and found that the association of RAC1<sup>Q61 L</sup>-MTOR was still progressively abrogated in a TNFAIP8L2-dose-dependent way by co-IP assay (Figure 4E). These data clearly suggested that TNFAIP8L2 blocks the association of RAC1 with MTOR in a dose-dependent way. Thus, it is reasonable to presume that TNFAIP8L2 can compete with MTOR for binding to RAC1 to impair MTOR activation.

To support this finding, we transfected plasmids to overexpress wild type TNFAIP8L2 or TNFAIP8L2<sup>K15,16Q</sup>, a mutation that decreases its binding ability with RAC1, along with the overexpressed MYC-RAC1 in HEK-293 T cells. Upon western blotting with the anti-MTOR antibody, a stronger MTOR signal using co-immunoprecipitation with RAC1 was detected with the TNFAIP8L2<sup>K15,16Q</sup> mutation, indicating that the disassociation of the TNFAIP8L2-RAC1 complex promotes RAC1-MTOR interaction (Figure 4F). As expected, when we restored the ability of TNFAIP8L2 to bind to RAC1, the MTOR signal decreased (Figure 4F). Overall, we propose that TNFAIP8L2 competes with MTOR for RAC1 binding and thereby enables the disassociation of the RAC1-MTOR complex.

### **TNFAIP8L2 suppresses the colocalization of active RAC1 and MTOR on the lysosome membrane by competitively binding to active RAC1**

RHEB conventionally activates the MTORC1 signaling in response to growth factors; subsequently, MTORC1 translocation to the lysosome membrane occurs through the RAG GTPase in response to amino acid stimulation [15,17,18,20]. The distribution of MTORC1 and its related factors in the lysosome membrane is thus intimately involved in MTORC1 activation. First, we observed that TNFAIP8L2 could reduce the colocalization of RAC1 and MTOR (Figure 5A), and its deficiency was shown to prompt MTOR and RAC1 colocalization in BMDMs in an immunofluorescent assay (Figure 5B).

TNFAIP8L2 can disrupt the interaction of RAC1 and MTOR, and the location of this interaction in the cell, especially in the lysosome membrane, is crucial for modulating MTOR signaling by TNFAIP8L2. Therefore, we sought to determine how the lysosomal distribution of RAC1 and MTOR is influenced by TNFAIP8L2 to clarify how MTOR activity is controlled downstream. We primarily observed that RAC1 could colocalize with MTOR in the lysosome membrane in HepG2 cells by immunofluorescence staining (Figure 5C). TNFAIP8L2 overexpression was shown to sharply decrease the colocalization of RAC1 and the lysosomal biomarker, LAMP1, whereas their colocalization was obviously increased in the absence of TNFAIP8L2 (Figure 5D and E). By isolating the lysosome component, we found that RAC1 was present in the lysosome (Figure 5F). Moreover, the levels of lysosomal RAC1 were decreased by TNFAIP8L2 (Figure 5G). Interestingly, we further found that TNFAIP8L2 was present in the LAMP1-positive structures (Figure 5G). As a result, TNFAIP8L2 decreases the RAC1 amounts in the lysosome.

We next sought to determine whether RAC1 translocation to the lysosome depended on its GTPase activity. We further expressed the GTPase-active RAC1<sup>Q61 L</sup> and GTPase-inactive RAC1<sup>T17 N</sup> mutations to determine their ability to translocate to the lysosomal membrane. The results showed that the lysosomal localization of active RAC1<sup>Q61 L</sup> was much higher than that of RAC1<sup>T17 N</sup>, indicating that RAC1 GTPase activity is required for its lysosomal translocation (Figure 5H). To further confirm this finding, we used the RAC1 GTPase inhibitor NSC-23766 to inhibit RAC1 activation and found that RAC1 lysosomal distribution was almost completely abolished (Figure 5I).

Although it has been reported that MTOR can bind to RAC1 independent of its GTP and GDP binding, we discovered that the translocation of RAC1 to the lysosome is dependent on its GTPase activity. To confirm our hypothesis, we determined the subcellular localization of RAC1 and MTOR. We found that their colocalization signals were significantly decreased and were dispersed from the nuclear periphery to the cytosol upon NSC-23766 treatment (Figure 5J).

Finally, we examined how the lysosomal distribution of p-MTOR was regulated by TNFAIP8L2 using MYC-RAC1<sup>Q61 L</sup>. The results showed that the lysosomal localization of p-MTOR was also gradually diminished with increasing TNFAIP8L2 (Figure 5K). However, we noticed that lysosomal MTOR loading was not affected by the overproduction of active RAC1 and TNFAIP8L2, indicating that the GTP binding of RAC1 did not affect MTOR translocation to the lysosome (Figure 5K). In summary, these data suggest that TNFAIP8L2 can block the RAC1-dependent MTOR activation by disrupting the interaction of active RAC1 with lysosomal MTOR to prevent lysosomal MTOR phosphorylation, rather than interfering with MTOR translocation to the lysosome.

### **Activation of MTORC1 is negatively regulated by TNFAIP8L2 by interacting with the GTP-binding RAC1**

Since TNFAIP8L2 can prevent lysosomal MTOR phosphorylation, we next determined how MTOR activity is influenced by TNFAIP8L2 through RAC1. MTOR reactivation was induced by serum re-stimulation for 20 min after 3 h of starvation in HepG2 cells (Figure 6A). We performed western blot analysis with an anti-p-MTOR and anti-p-RPS6 antibody, an MTOR downstream signal, to evaluate MTOR activity by overexpressing Flag-TNFAIP8L2. Compared to the cells grown in normal growth conditions, the phosphorylation of MTOR and RPS6 were inhibited under starvation (Figure 6A and S4A). However, different levels of p-MTOR and p-RPS6 were observed, depending on the TNFAIP8L2 level, upon returning from starved cells to normal growth conditions. We found that TNFAIP8L2 decreased MTOR and RPS6 phosphorylation in response to serum re-stimulation after starvation for 3 h in both cell lines (Figure 6A and S6A).

Conversely, when we utilized *Tnfaip8l2*-deleted BMDMs or HeLa cells with downregulated *TNFAIP8L2* using small RNA interference, MTOR activities were both increased upon serum supplementation after starvation, as illustrated by RPS6 phosphorylation (Figure 6B and S4B). Furthermore,

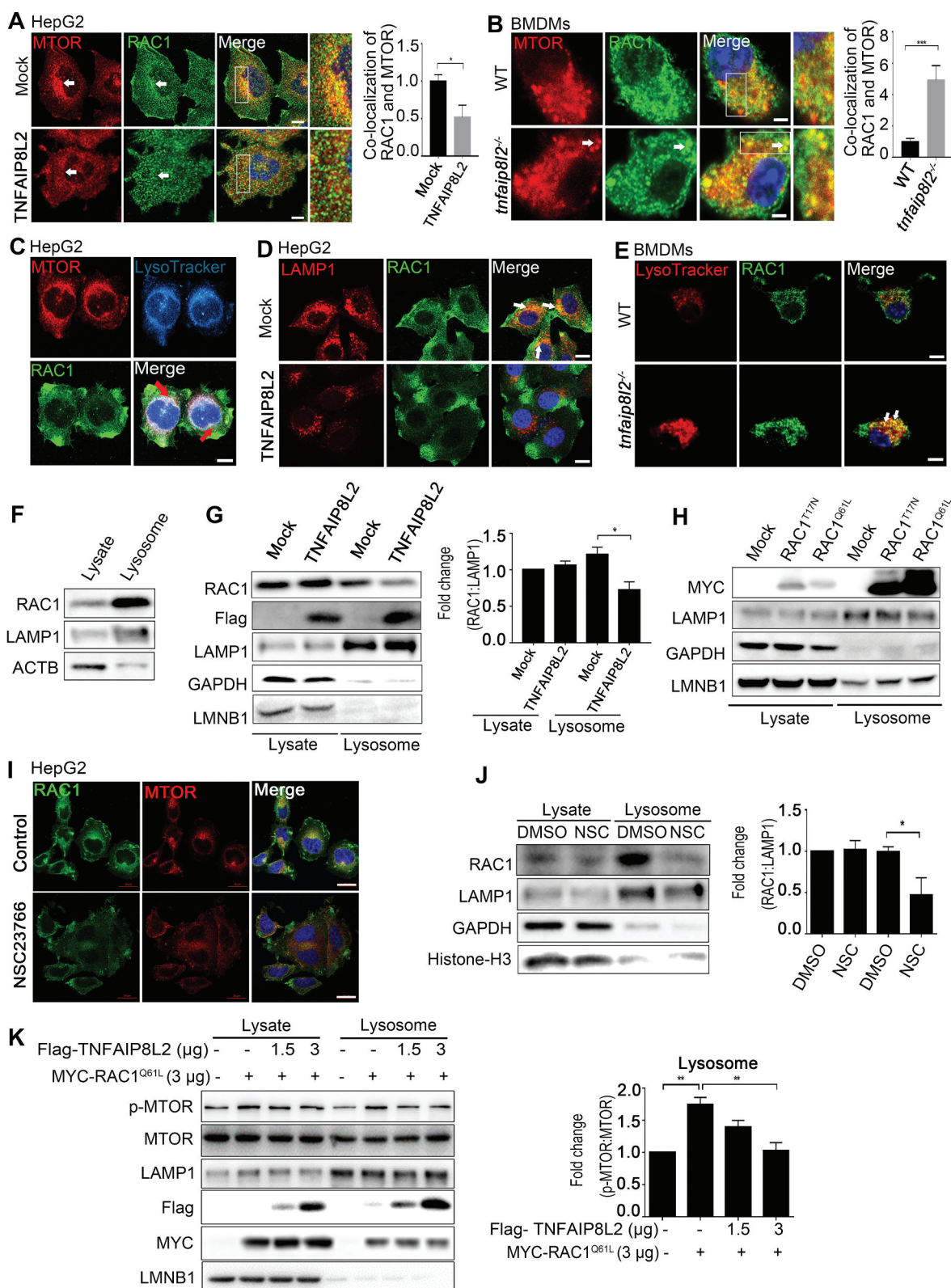


**Figure 5.** TNFAIP8L2 suppresses the colocalization of active RAC1 and MTOR on the lysosome membrane by competitively binding to active RAC1. HepG2 cells with or without overexpressing Flag-TNFAIP8L2 (A) and BMDMs (B) were fixed and immunostained for anti-MTOR antibody (red) and anti-RAC1 antibody (green), and further analyzed by confocal microscopy. Arrows denote the colocalized puncta of RAC1 and MTOR. The scale bar sizes are 5  $\mu$ m for (A) and 10  $\mu$ m for (B). The quantitative analysis of the colocalization of RAC1 and MTOR was performed by IPP software. Average value in HepG2 without TNFAIP8L2 overexpression in control or WT BMDMs without any treatment was normalized to 1. Values are mean  $\pm$  SEM ( $n \geq 20$ ). (C) Subcellular localization of RAC1, MTOR, and LysoTracker Red marked the lysosome in HepG2 cells. The signals of RAC1 and MTOR were analyzed by confocal microscopy after immunostaining with their antibodies. Scale bars: 5  $\mu$ m. (D) The HepG2 cells with or without overexpressing Flag-TNFAIP8L2 were fixed and immunostained with anti-RAC1 and anti-LAMP1 antibodies before being analyzed by confocal microscopy. Scale bars: 10  $\mu$ m. (E) BMDMs from WT or *Tnfaip8l2*-deficient mice were stained with LysoTracker Red for 1 h, fixed, and then immunostained with an anti-RAC1 antibody. The fluorescent signals were observed by immunofluorescence microscopy. Scale bars: 10  $\mu$ m. (F) Lysosome isolations in HEK-293 T cells



we observed that RPS6 phosphorylation was remarkably enhanced even in complete medium when TNFAIP8L2 was deficient or downregulated (Figure 6B and S4B). Using immunofluorescence assay with p-RPS6 antibody, overexpression of TNFAIP8L2 reduced the p-RPS6 signals, and the loss of TNFAIP8L2 enhanced MTOR activity upon serum re-stimulation (Figure 6C and D). During serum re-stimulation, more than a 2-fold increase in MTOR activity was detected by a quantitative calculation of the p-RPS6-positive signals from the immunofluorescence images of *Tnfaip8l2*-deficient BMDMs (Figure 6D). Together, these data provide evidence that TNFAIP8L2 could negatively modulate MTOR activity.

Then, we sought to ask whether the regulation of MTOR by TNFAIP8L2 is dependent on RAC1 since TNFAIP8L2 can prevent the association between active RAC1 and MTOR on the lysosomal membrane. First, we designed an experiment to block RAC1 GTPase activity in HepG2 cells and observed that the p-RPS6 level decreased in response to NSC-23766 treatment compared to DMSO-treated cells as a control (Figure 6E). By overexpressing wild type RAC1, RAC1<sup>T17N</sup>, or RAC1<sup>Q61L</sup> separately, we found that RPS6 phosphorylation was inhibited in serum starvation conditions independent of the RAC1 GTPase. However, the p-RPS6 level positively correlated to RAC1 GTPase activity upon serum supplementation in both HepG2 and BEL-7402 cell lines (Figure 6F and S5). These results revealed that RAC1 GTPase activity is required for MTORC1 activation.

In the absence of TNFAIP8L2, RAC1<sup>Q61L</sup> showed a higher ability to promote RPS6 phosphorylation under normal culture conditions, serum starvation, and serum re-stimulation in both HepG2 and BEL-7402 cell lines (Figure 6G and S6A). TNFAIP8L2 abolished the enhanced MTOR phosphorylation induced by active RAC1 upon serum re-stimulation (Figure 6G and S6A). An increase of p-RPS6 levels was observed by TNFAIP8L2<sup>K15,16Q</sup> in RAC1<sup>Q61L</sup>-overexpressing cells upon serum re-stimulation (Figure 6H and S6B). Moreover, TNFAIP8L2<sup>K15,16Q</sup> decreased both LC3B-II and SQSTM1 levels and abolished wild type TNFAIP8L2-induced autophagy dysfunction, suggesting that TNFAIP8L2<sup>K15,16Q</sup>-induced recovery of MTOR activation improved autophagy flux (Figure 6I). As a result, TNFAIP8L2 was further confirmed to target active RAC1 to inhibit MTORC1 activation, and ultimately prevent the phosphorylation of RPS6.

Here, our data support the notion that TNFAIP8L2 could bind to the lysosomal GTP-bound RAC1 to negatively regulate MTOR activity. However, MTOR translocation to the

lysosome is not influenced by TNFAIP8L2 (Figure 5K). As for MTOR activity regulation, GTP-bound RAC1 is supposed to be the direct target for TNFAIP8L2.

### **TNFAIP8L2 deficiency exacerbates inflammation by the upregulation of MTOR activity in an LPS-induced endotoxemia model**

MTOR activity is closely associated with inflammation, and its upregulation can promote inflammatory responses [39,40]. To evaluate whether the anti-inflammatory role of TNFAIP8L2 depends on the MTORC1 pathway, we generated *tfaip8l2* knockout mice using CRISPR-Cas9 as described in the Methods. In macrophages, *Tnfaip8l2* deficiency exacerbated inflammatory responses by increasing pro-inflammatory cytokines IL6 and TNF upon the activation of the Toll-like receptor pathway by lipopolysaccharide (LPS) stimulation. At the same time, the increased IL6 and TNF were markedly attenuated by blocking MTOR activity with rapamycin (Figure 7A and B). This result indicated that TNFAIP8L2 might control inflammation by modulating MTOR activity.

We further measured the MTOR activity by blotting for p-MTOR and its downstream signal, p-RPS6. Compared to wild type mice, *Tnfaip8l2* deficiency led to higher levels of p-MTOR and p-RPS6 in macrophages in the absence and presence of LPS stimulation and the rapamycin treatment obviously abrogated the increase of p-MTOR and p-RPS6 (Figure 7C). Thus, it is conceivable for us to conclude that *Tnfaip8l2* deficiency can promote inflammatory responses by upregulating MTOR activity.

Furthermore, in the LPS-induced endotoxemia model, we found that circulating pro-inflammatory cytokines IL6 and TNF levels in plasma were also enhanced in *Tnfaip8l2*-deficient mice compared with wild type mice, and these increases were almost eliminated by rapamycin (Figure 7D and E). The *Tnfaip8l2*-deficient mice showed the lowest body temperature while inhibiting MTOR activity could alleviate this effect (Figure 7F).

By hematoxylin and eosin (HE) and immunohistochemistry staining of lung tissues, we evaluated tissue inflammation by measuring both the number of infiltrated immune cells and MTOR activity by evaluating the p-RPS6 expression. We found *Tnfaip8l2* deficiency exacerbated the infiltration of inflammatory cells and enhanced p-RPS6 expression in lung tissues, whereas rapamycin inhibited MTOR activity and attenuated inflammation (Figure 7G and 7H). In summary, *Tnfaip8l2* deficiency can exacerbate inflammatory responses by upregulating MTOR activity.

were performed according to the manufacturer's instructions. The levels of RAC1, LAMP1, and ACTB in whole-cell lysates and lysosome lysates were analyzed by western blotting. (G) HEK-293 T cells were transfected with empty vector and *Flag-TNFAIP8L2* plasmids. The levels of RAC1, TNFAIP8L2, LAMP1, GAPDH, and LMNB1 in whole-cell and lysosome lysates were analyzed using western blotting. The quantifications of RAC1 were performed. (H) HEK-293 T cells were transiently transfected with *MYC-RAC1<sup>T17N</sup>* and *RAC1<sup>Q61L</sup>*. Levels of MYC-RAC1<sup>T17N</sup> and MYC-RAC1<sup>Q61L</sup>, LAMP1, GAPDH, and LMNB1 in cell and the lysosome lysates were analyzed by western blotting. (I) HEK-293 T cells were treated with or without RAC1 inhibitor NSC23766 (100 nM) for 6 h. RAC1, TNFAIP8L2, LAMP1, GAPDH and Histone-H3 in the whole-cell and lysosome lysates were measured by western blotting. (J) The subcellular localization of RAC1 and MTOR in response to RAC1 inhibitor NSC23766 (100 nM) were observed by confocal microscopy after immunostaining with anti-RAC1 antibody, anti-MTOR antibody, and DAPI. Scale bars: 20  $\mu$ m. (K) HEK-293 T cells were transfected with *MYC-RAC1<sup>Q61L</sup>* with the increasing *Flag-TNFAIP8L2* plasmids (0, 1.5, and 3  $\mu$ g) and lysosome isolations were performed. The levels of total MTOR, p-MTOR, LAMP1, Flag, MYC, and LMNB1 in whole-cell and lysosome lysates were determined by western blotting with their antibodies correspondingly. Band intensity quantifications of RAC1 (G and J) and p-MTOR (K) were performed by Photoshop software. Average value in vector-transfected cells (G, J, K) without any treatment was normalized as 1. Values are mean  $\pm$  SEM (n = 3), Statistical analysis was performed using Student's t-test analysis in (G, I, J): \*p < 0.05, \*\*p < 0.01, \*\*\*p < 0.001.

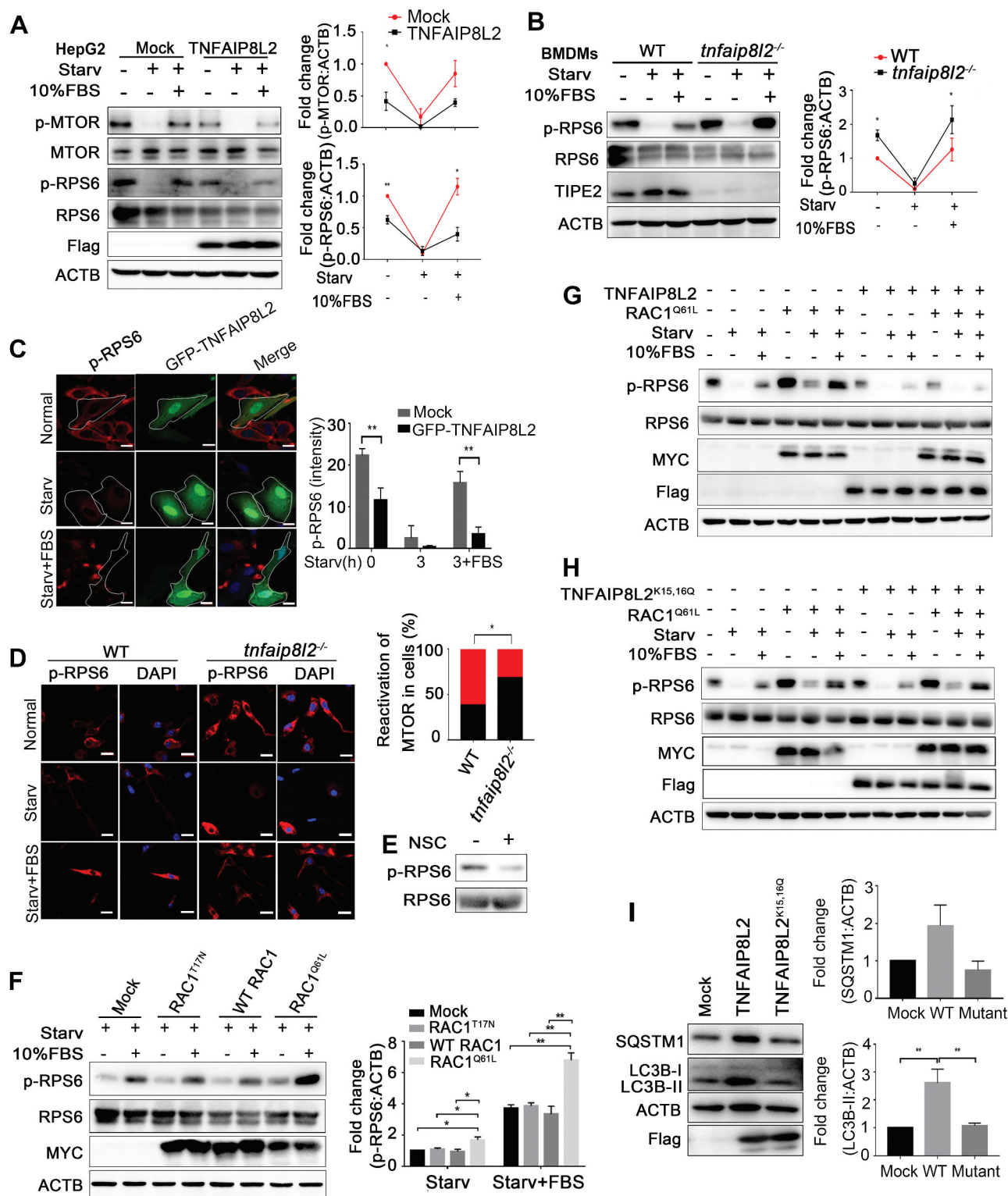


**Figure 6.** MTORC1 activation is negatively regulated by TNFAIP8L2 through interacting with the GTP-binding RAC1. HepG2 cells with the empty vector or *Flag-TNFAIP8L2* plasmids (A) and BMDMs from WT and *Tnfaip8l2*-deficient mice (C) were re-stimulated with or without 10% FBS for 20 min after starvation for 3 h. The total MTOR and RPS6, p-MTOR and RPS6, Flag and ACTB were determined by western blotting. The quantitative analyses of p-MTOR and p-RPS6 signals were performed by Photoshop software. Values are mean  $\pm$  SEM (n = 3). Average value in vector-transfected cells or WT BMDMs without any treatment was normalized to 1. HepG2 cells with or without overexpressing *Flag-TNFAIP8L2* (B) and BMDMs from WT and *Tnfaip8l2*-deficient mice (D) were treated as in (A) and stained with p-RPS6 antibodies and DAPI. The quantitative analysis of p-RPS6 signals and the number of reactivation or un-reactivation cells were measured by using Zeiss Automeasure software. Scale bars: 10  $\mu$ m (B), 20  $\mu$ m (D). Values are mean  $\pm$  SEM (n  $\geq$  20). (E) HepG2 cells were treated with 100 nM NSC23766 for 6 h. Total RPS6 and p-RPS6 were analyzed by western blotting. (F) HepG2 cells were transfected with control vector, or WT *MYC-RAC1*, *MYC-RAC1<sup>T17N</sup>*, and *MYC-RAC1<sup>Q61L</sup>* plasmids for 24 h. Then cells were re-stimulated with or without 10% FBS for 20 min after starved for 3 h. Total RPS6 and p-RPS6 were determined by western blotting. The quantitative analysis of p-RPS6 signals was performed by Photoshop software. Values are mean  $\pm$  SEM (n = 3). Average value in vector-transfected cells with starvation was normalized to 1. (G) HepG2 cells were transfected with *Flag-TNFAIP8L2* or *MYC-RAC1<sup>Q61L</sup>* alone and both. Cells were re-stimulated for 20 min by 10% FBS in DMEM after starved for 3 h. The levels of p-RPS6, RPS6, MYC-RAC1, *Flag-TNFAIP8L2*, and ACTB were analyzed by western blotting. (H) HepG2 cells were transfected with *Flag-TNFAIP8L2<sup>K15,16Q</sup>* or *MYC-RAC1<sup>Q61L</sup>* alone and both. Cells were treated as in (G). (I) HepG2 cells were transfected with WT *Flag-TNFAIP8L2* or *Flag-TNFAIP8L2<sup>K15,16Q</sup>* for 24 h. The levels of SQSTM1, LC3B-I/II, and ACTB were analyzed by western blotting. The quantitative analysis of SQSTM1 and LC3B-I/II signals was performed the same as in (F). Statistical analysis was performed using Student's t-test (D, I) and two-way ANOVA (A-C, F) analysis: \*p < 0.05, \*\*p < 0.01.

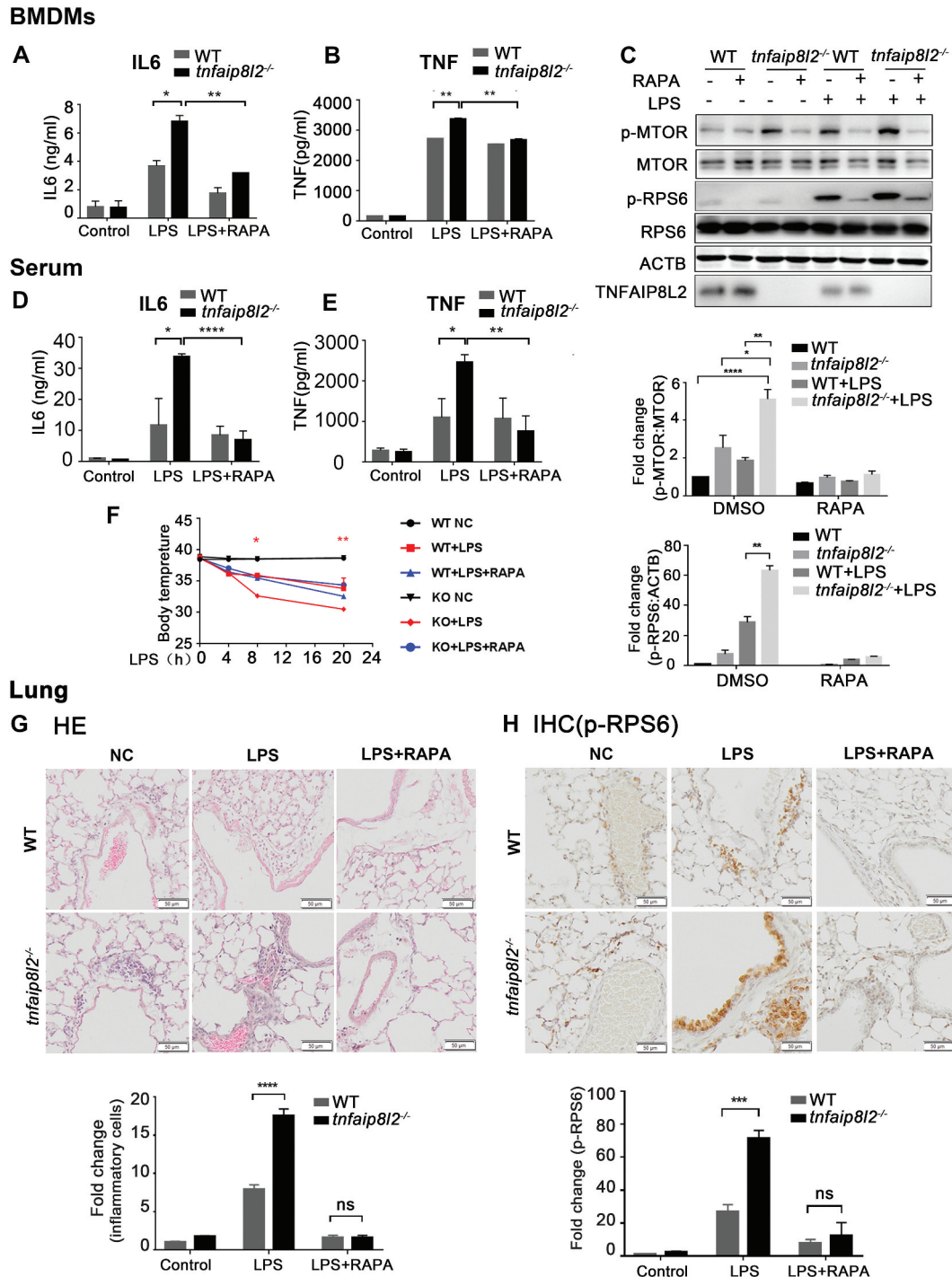


**Figure 7.** *Tnfaip8l2* deficiency exacerbates inflammation by the upregulation of MTOR activity in LPS-induced endotoxemia mice. Macrophages from WT and *Tnfaip8l2*-deficient mice ( $n = 3$ ) were treated with or without rapamycin ( $5 \mu\text{M}$ ) for 6 h before treatment with LPS ( $100 \text{ ng/ml}$ ) for 4 h. IL6 (A) and TNF (B) concentrations in the cell culture supernatant were determined by ELISA. (C) The phosphorylation and total of MTOR and RPS6 in macrophages with the same treatment as in (A) were measured by western blotting. Band intensity quantifications of p-MTOR and p-RPS6 were performed by Photoshop software. Average value in WT BMDMs without any treatment was normalized as 1. (D-H) WT and *Tnfaip8l2*-deficient littermates were injected intraperitoneally with a low-dose of LPS ( $10 \text{ mg/kg}$ ) for 24 h after 8 h RAPA ( $2 \text{ mg/kg}$ ) treatment. The levels of IL6 (D) and TNF (E) in serum were determined by ELISA. (F) Mice body temperature was measured at 0, 4, 8, and 20 h after LPS injection.  $p$ -value means the significant differences of body temperature between WT+LPS group and *tnfaip8l2*<sup>-/-</sup> + LPS group. Values are mean  $\pm$  SEM ( $n = 3$ ). Lung sections from WT and *Tnfaip8l2*-deficient mice were stained with hematoxylin and eosin (G) and anti-p-RPS6 antibody (H). The quantitative analysis was performed by IPP software. Average value in WT group without any treatment was normalized to 1. Two-way ANOVA analysis was performed in (A-H): \* $P < 0.05$ ; \*\* $P < 0.01$ ; \*\*\* $P < 0.001$ ; \*\*\*\* $P < 0.0001$ . Values are mean  $\pm$  SEM ( $n = 3$ ). Scale bars:  $50 \mu\text{m}$ .

## Discussion

Our studies support a molecular mechanism for the impairment of ALR by TNFAIP8L2 in glutamine- and serum starvation-induced autophagy by repressing MTOR reactivation by modulating the RAC1-MTORC1 axis. MTOR signaling is intimately related with autophagy and is inhibited during autophagy initiation, but is reactivated sequentially during ALR under prolonged starvation [30–32]. Reactivation of MTOR has been illustrated to be indispensable for autophagy activation. Here, we determined TNFAIP8L2, previously as a negative regulator of immunity, can repress MTOR reactivation upon prolonged starvation, thereby leading to defects in ALR and consequently impairing autophagy flux. Additionally, TNFAIP8L2 is physiologically involved in anti-inflammation by negatively modulating MTOR activity in an LPS-induced mouse model of endotoxemia.

We investigated the mechanism underlying regulation of MTORC1 activity by TNFAIP8L2 to influence ALR in starvation-induced autophagy. A previous study illustrates that TNFAIP8L2/TIPE2 can bind directly to the C-terminal CAAX motif of RAC1 and block its GTPase activity and RAC1-dependent signaling [14]. In addition, the C-terminus of RAC1 is necessary for interacting with MTOR to regulate both MTORC1 and MTORC2 activity. We, therefore, investigated whether TNFAIP8L2 modulates MTOR activity in a RAC1-dependent manner. Indeed, our studies revealed that TNFAIP8L2 could compete with MTOR for binding to RAC1 by co-IP analysis.

There is a consensus that the localization of MTORC1 to the lysosomes is critical for its ability to sense and respond to variations in amino acid levels [15,17–20,41–43]. Further, we observed that active RAC1 is preferentially translocated to the lysosomal membrane to interact with lysosomal MTOR, whereas both GTP- and GDP-bound RAC1 can bind to MTOR as previously reported [14]. We additionally found that TNFAIP8L2 can disassociate active RAC1 from the lysosomal RAC1-MTORC1 complex by binding to RAC1 competitively, thereby facilitating the inhibition of MTORC1 signaling. As previously reported, TNFAIP8L2 can inhibit RAC1 GTPase activity and it can be speculated that TNFAIP8L2 may inhibit active RAC1 in the cytoplasm to disrupt active cytoplasmic RAC1 translocation to the lysosomal membrane and eventually repress lysosomal MTOR activation. However, we identified that the release of active RAC1 from the lysosome membrane mediated by TNFAIP8L2 provides a novel role for TNFAIP8L2 in negatively regulating the MTORC1 signaling. In this respect, some issues need to be resolved. Since we found that TNFAIP8L2 can be localized to the lysosome, the differences between cytoplasmic and lysosomal TNFAIP8L2 in regulating lysosomal RAC1-MTORC1 complex should be further clarified. In turn, further studies should also examine what happens to lysosomal TNFAIP8L2 when active RAC1 disassociates from the lysosome membrane.

Notably, we observed that active RAC1 differs from RAG GTPase in that it cannot influence MTOR translocation to the lysosome membrane. Future studies should examine what stimulates the translocation of RAC1 to the lysosome. Whether RAC1 is responsive to amino acid signaling is still

unclear. However, it appears that RAC1 activates MTORC1 in a GTPase-dependent manner, similar to RHEB.

Since TNFAIP8L2 can inhibit MTORC1 activity as described above, it is reasonable to hypothesize that TNFAIP8L2 would induce autophagy. During autophagy initiation, we observed that TNFAIP8L2 could promote autophagy, as expected. However, we found that TNFAIP8L2 impaired autophagy flux under starvation conditions by interfering with ALR. Therefore, TNFAIP8L2 could be a novel therapeutic target for diverse disorders caused by defective autophagy, including neurodegeneration, cancer, heart disease, cardiomyopathies, and infectious diseases [29,44]. MTORC1 activation has emerged as a central pathway for the pathogenesis of obesity, systemic lupus erythematosus, and other autoimmune diseases. By blockage of MTOR, TNFAIP8L2 can also function as a promising target to protect organisms against these diseases [45].

In this study, we focused on examining the effects of TNFAIP8L2 on the metabolic sensing effector MTORC1 to control autophagy. However, PtdIns(4,5)P<sub>2</sub> can recruit clathrin and KLF5B to autolysosomes and is required for ALR after prolonged starvation [46,47]. Importantly, TNFAIP8L2 has been shown to directly interact with PtdIns(4,5)P<sub>2</sub> and can extract it from the lipid bilayer and transfer it to the aqueous solution [11,48,49]. Therefore, it is reasonable to speculate TNFAIP8L2 can probably reduce the PtdIns(4,5)P<sub>2</sub> distribution on the lipid bilayer to directly disrupt autolysosome tubulation during ALR. This hypothesis is very interesting because there is no evidence to show any immunological factors in the direct regulation of ALR. Of course, we cannot exclude this possibility in our study as well. Therefore, this direction needs to be investigated further. Collectively, TNFAIP8L2 is presented to be a novel and protective role for organisms to inhibit inflammation through negatively modulating MTORC1 activity. However, upon prolonged nutrient deficiency, TNFAIP8L2 can impair ALR through MTORC1 and lead to cell death. How TNFAIP8L2 balances these two biological processes requires further investigation.

## Materials and methods

### Antibodies and reagents

The antibodies used for this study were: TNFAIP8L2 (TNFAIP8L2/TIPE2; Proteintech, 15940-1-AP), SQSTM1/p62 (Abcam, ab109012), RAC1 (Abcam, ab33186), Flag (Medical & Biological Laboratories, M185-3 L), MYC (Origene, TA150121), isotope control antibody IgG (R&D systems, MAB004), ACTB/ $\beta$ -actin (ORIGENE, TA-09), GAPDH (ZSGB-Bio, OTI2D9) and LMNB1 (lamin B1; Proteintech, 66095-1-1 g). The following antibodies were purchased from Cell Signaling Technology: LAMP1 (3243), p-RPS6/S6 (Ser235/236; 4858), RPS6/S6 (2217), p-MTOR (Ser2448; 5536), MTOR (2983), LC3B (3868) and RHEB (13879). Horseradish peroxidase-conjugated secondary antibodies were from Abcam: anti-rabbit IgG Alexa Fluor 488 (ab181448), anti-mouse IgG Alexa Fluor 488 (ab150117), anti-rabbit IgG Alexa Fluor 594 (ab150088) and anti-rabbit IgG Alexa Fluor 647 (ab150075). Other reagents used in this study were: LysoTracker Red (Beyotime-Biotechnology, C1046), FVD eFluor 660

(eBioscience, 65–0864), bovine serum albumin (BSA; Sigma Aldrich, V900933), RIPA cell lysis buffer (50 mM Tris-HCl, pH 7.4, 150 mM NaCl, 1% NP-40 [Beyotime, P0013D]) and NSC-23766 (Selleckchem, 2321084). Protein mass marker was a mixture of proteins from 10 kDa to 170 kDa (Thermo Fisher Scientific, 26617). Anti-MYC magnetic beads (Bimake, B26301), bafilomycin A<sub>1</sub> (BafA<sub>1</sub>; Sigma Aldrich, B1793), rapamycin (MCE, HY-10219) and Lysosome isolation kit were from BestBio (BB-3603-1), mouse IL6/IL-6 ELISA MAX Standard Set (B183449) and mouse TNF/TNF- $\alpha$  ELISA MAX Standard Set (B430904) were from BioLegend. Xylene and alcohol (Sinopsin group chemical reagent co. LTD), phosphate-buffered saline (Solarbio life sciences, p1010) were from the indicated sources. Tween-20 (Sigma Aldrich, P1379), EDTA (Sigma Aldrich, E9884), HEPES (Sigma Aldrich, 83264), beta-glycerophosphate, (Sigma Aldrich, G90422), CHAPS (Sigma Aldrich, C9426), PMSF (Sigma Aldrich, 10837091001), leupeptin (Sigma Aldrich, L2884), aprotinin (Sigma Aldrich, A1153), normal goat serum (Jackson ImmunoResearch, 005–000-121).

### Cell lines and cell culture

HepG2, HEK-293 T, HeLa, H1975 and BEL-7402 cell lines were purchased from Shanghai Cell Bank of Chinese Academy of Sciences (SCSP-510; GNHu17; TCHu187; SCSP-597; TCHu10, respectively) and grown in DMEM medium (Gibco, 12100046) supplemented with 10% heat-inactivated fetal bovine serum (FBS; Gibco, 10099–141). Cells were all cultured in a humidified cell incubator with an atmosphere of 5% CO<sub>2</sub> at 37°C. Starvation medium is DMEM medium (BasalMedia, L150 KJ) without the supplementation of serum and glutamine.

### Plasmids, siRNA, adenovirus and transfection

Human WT *TNFAIP8L2* and *RAC1* were generated from the genomic cDNA by PCR and then cloned into vector pRK5 with a C-terminal Flag. Vector pRK5 was a gift from Yongyu Shi (Shandong University, China). The *TNFAIP8L2*<sup>K15,16Q</sup> mutant, in which lysine 15, 16 and arginine 24 were replaced with glutamine and alanine, separately. The mutants were generated using PCR-based site-directed mutagenesis. All the *RAC1* mutants were generated from the *RAC1* plasmid using the KOD-Plus-Mutagenesis kit (Toyobo CO., LD, SMK-101). Control siRNA and siRNA against *TNFAIP8L2* were purchased from Genepharma.

siRNA1: 5'-CAGGAAGCTGCTAGACGAA-3';

siRNA2: 5'-GCCACGTGTTTGATCACTT-3';

siRNA3: 5'-GCTGCTAGAGTTGGTGGAA-3';

control siRNA: 5'-AGTGAAACAGTGCAGCTGC-3'.

Plasmids and siRNA were transfected to cells by using Lipofectamine 2000 (Invitrogen, 11668019) according to the manufacturer's protocol.

### Transfection of adenovirus and analysis

*mCherry-EGFP-Lc3b* adenovirus infection of HepG2 cells was performed according to the manufacturer's protocol (ViGene Biosciences, multiplicity of infection = 10–50,  $1.0 \times 10^9$  plaque-

forming units/ml). The fluorescence signals were observed by laser confocal scanning microscope. We analyzed mCherry-positive and EGFP-negative vesicles (red puncta) and both mCherry- and EGFP-positive vesicles (yellow puncta). The number of red and yellow spots was calculated by IPP software. The average value in vector-transfected cells without any treatment was normalized to 1. Graphpad prism 7 software was used to perform statistical analyses.

### Generation of *Tnfaip8l2*-deficient mice

C57BL/6 (B6) mice were obtained from the Vital River Laboratory Animal Technology Company (Beijing, China) and housed at a specific pathogen-free environment. *Tnfaip8l2*-deficient mice were generated through the CRISPR-Cas9 system to delete *Tnfaip8l2* exon 2 by Beijing Biocytogen Co.Ltd. (sgRNA sequence: sgRNA1:GCTTGTCACCCATATGAAGTTGG; sgRNA2:ACCAATGCTTCTCGATCCCCTGG). Genotype identifications were in supplemental materials as shown in Figure S2A. Littermate controls referred to *tnfaip8l2*<sup>-/-</sup> and WT mice were used for experimental analysis.

### Endo-toxic shock model

Littermate controls referred to WT and *Tnfaip8l2*-deficient mice were used *in vivo* experiments. For endotoxic shock model, 10-week male mice were injected intraperitoneally with 10 mg/kg LPS (Sigma Aldrich, E. coli 055: B5) after injection of rapamycin (RAPA) for 6–8 h. The body temperature of mice was monitored by an infrared electronic thermometer (CEM, DT-8806 S) at 0, 4, 8, and 20 h after LPS treatment. WT and *Tnfaip8l2*-deficient mice were anesthetized after LPS treatment for 24 h. The serum and lung tissue were used for cytokine expression analysis, H&E, and IHC experiment. All animal experiments were undertaken in accordance with the National Institute of Health Guide for Care and Use of Laboratory Animals.

### Histology and immunohistochemistry

Paraffin-embedded lung tissue sections from WT and *Tnfaip8l2*-deficient mice (n = 3/group) were stained with hematoxylin and eosin (H&E). The expression of p-RPS6 of lung tissue section WT and *Tnfaip8l2*-deficient mice (n = 3/group) was detected by immunohistochemistry staining. Section was dewaxed and hydrated, followed by antigen retrieval [50]. Endogenous peroxidase was blocked by 3% hydrogen peroxide solution. The section was incubated with the blocking goat serum for 15 min and immunostained with anti-p-RPS6 overnight at 4°C. After three washes with phosphate-buffered saline (PBS; KH<sub>2</sub>PO<sub>4</sub> 2 mM, Na<sub>2</sub>HPO<sub>4</sub> 8 mM, NaCl 136 mM, KCl 2.6 mM, pH 7.2 ~ 7.4) buffer, the slides were stained with horseradish peroxidase-conjugated anti-rabbit IgG and 3, 5-diaminobenzidine peroxidase Substrate Kit (ZSGB-BIO, ZLI-9017), followed by counterstaining with Mayer's hematoxylin. The full section was scanned by using the Panoramic Scanning Microscope-VS120 (Olympus Life Science), and 5 fields per section at 100x magnification were randomly selected. The number of the infiltrated immune

cells, including polymorphonuclear granulocyte, mononuclear macrophages, and lymphocytes were counted according to their morphology and size by using Image Pro Plus (IPP) software and calculated the mean value. The density of p-RPS6-positive staining (brownish yellow) was analyzed by IPP software [51,52].

### **BMDMs isolation and culture**

To generate bone marrow-derived macrophages (BMDMs), bone marrow cells were harvested from mice and cultured for 6 d in 100 ng/ml M-CSF (PEPROTECH, AF-300-25). In accordance with the routine culture, fresh medium and cytokine were added on the third day [14]. Cells were washed twice with cold PBS buffer, resuspended in DMEM with 10% FBS and rested for 24 h before analysis.

### **Immunofluorescence and confocal microscopy**

Predisposed cells were seeded on glass coverslips and cultured in DMEM with 10% serum. Cells were then washed with PBS and fixed in the stationary liquid from Beyotime Biotechnology (Shanghai, China) for 10 min. They were blocked with 2% BSA for 60 min and stained with primary antibodies overnight at 4°C. After three washes with PBS buffer, cells were incubated with horseradish peroxidase-conjugated secondary antibody for 1 h. The fluorescence of antibody signals was visualized using Alexa Fluor 647-, Alexa Fluor 488- or Alexa Fluor 594-conjugated IgG (Abcam). DAPI (Beyotime-Biotechnology) was used to stain the nucleus for 10 min. Images were captured by a confocal laser scanning microscope (Carl Zeiss, LSM780, Oberkochen, Germany) with a 63 x Plan-Apochromat objective and were analyzed using ZEN lite 2012 software package. All statistical image analysis was performed using Image Pro-Plus Software and Zeiss Auto-measure software. We statistically analyzed the percentage of p-RPS6-positive cells in which the p-RPS6 fluorescence signal was significantly increased after 10% FBS retreatment for 20 min or starvation ( $n \geq 20$  cells in each sample).

### **ELISA**

The concentrations of mouse IL6, TNF were detected using ELISA MAX™ Standard Sets (Biolegend, B183449; B430904) according to the manufacturer's instruction.

### **Western blotting**

Cells were lysed with RIPA cell lysis buffer with 1% protease inhibitor cocktail (Bimake, B14002). Followed by high-speed (12,000 x g) centrifugation for 30 min at 4°C, the supernatant was collected, and its concentration was measured using a BCA method. 10–30 µg of denatured protein was separated by 8%, 10% or 12% SDS-PAGE, and then transferred to PVDF membranes (Millipore, IPVH00010). The membranes were blocked with 5% bovine serum albumin (BSA) in TBS-T (Tris-buffered saline Tween 20) for 2–3 h and incubated with primary antibodies overnight at 4°C, followed by horseradish peroxidase-conjugated secondary antibodies incubation for 1 h. After 3

washes with TBS-T, signals were detected by the ECL detection system (Sage Creation Science, MiniChemi 500). The specific bands were analyzed using an eECL Western Blot Kit (Millipore, 69078). All protein signals were collected with different exposure time to make sure the bands were not overexposed and within the linear range to perform quantitative analysis.

### **Co-immunoprecipitation**

HEK-293 T cells were lysed using the co-immunoprecipitation (IP) buffer (120 mM NaCl, 1 mM EDTA, 40 mM HEPES, pH 7.4, 50 mM NaF, 10 mM beta-glycerophosphate, 0.3% CHAPS, 1 mM Na<sub>3</sub>VO<sub>4</sub>, 1 mM PMSF, 10 mg/ml leupeptin, 10 mg/ml aprotinin, and 10 mM MgCl<sub>2</sub>). Lysates were centrifuged at 12,000 x g for 30 min at 4°C and incubated with primary antibody for 1 h. Protein A/G-Sepharose (Santa Cruz Biotechnology, sc-2003) was added and incubated overnight at 4°C with rotation. Then the protein complexes were washed 5 times with IP buffer and boiled for 5 min, followed by SDS-PAGE and western blotting analysis.

### **Flow cytometry**

Cells were grown in DMEM medium without serum and glutamine and starved to death for the indicated times. FVD eFlour 660 were used to stain dead cells and cell death was analyzed by flow cytometry.

### **Lysosome isolation**

We isolated the lysosome component by the Lysosome isolation kit. Briefly, about  $1-2 \times 10^7$  cells were collected and washed 3 times with PBS buffer. Then cells were homogenized and lysosomes were purified by gradient centrifugation.

### **Statistical analysis**

The quantifications of western blotting and the fluorescent signals in immunofluorescence images were performed. Differences were analyzed using the Student's t-test or two-way ANOVA for variables. P-values < 0.05 were considered to be statistically significant. Statistical analyses were carried out using GraphPad Prism7, and statistical data are presented as mean ± SEM.

### **Acknowledgments**

We thank Professor Yingyu Chen (Department of Immunology, Peking University School of Basic Medical Sciences) and all Lining Zhang's lab members for their discussions and comments. We are also very grateful to Professor Youhai H. Chen (Department of Pathology and Laboratory Medicine, University of Pennsylvania) for kindly providing the RAC1 and TNFAIP8L2 expression plasmids.

### **Disclosure statement**

No potential conflict of interest was reported by the authors.

## Funding

This research is supported by the National Key Research and Development Program of China [No.2016YFC1303400]; the National Natural Science Foundation of China [81971471, 31470856 and 81771775]; the Shandong Provincial Key Research and Development Program [2019JZZY011113]; Shandong Provincial Natural Science Foundation [2014GSF118076, ZR2011HZ003] and the Fundamental Research Funds of Shandong University [2014QY004].

## ORCID

Yetong Guan  <http://orcid.org/0000-0002-9665-8303>

## References

- [1] Deretic V, Saitoh T, Akira S. Autophagy in infection, inflammation and immunity. *Nat Rev Immunol.* 2013;13(10):722–737.
- [2] Levine B, Mizushima N, Virgin HW. Autophagy in immunity and inflammation. *Nature.* 2011;469(7330):323–335.
- [3] Pilli M, Arko-Mensah J, Ponpuak M, et al. TBK-1 promotes autophagy-mediated antimicrobial defense by controlling autophagosome maturation. *Immunity.* 2012;37(2):223–234.
- [4] Harris J, De Haro SA, Master SS, et al. T helper 2 cytokines inhibit autophagic control of intracellular mycobacterium tuberculosis. *Immunity.* 2007;27(3):505–517.
- [5] Sun H, Gong S, Carmody RJ, et al. TIPE2, a negative regulator of innate and adaptive immunity that maintains immune homeostasis. *Cell.* 2008;133(3):415–426.
- [6] Zhang Y, Wei X, Liu L, et al. TIPE2, a novel regulator of immunity, protects against experimental stroke. *J Biol Chem.* 2012;287(39):32546–32555.
- [7] Cao X, Zhang L, Shi Y, et al. Human tumor necrosis factor (TNF)-alpha-induced protein 8-like 2 suppresses hepatocellular carcinoma metastasis through inhibiting Rac1. *Mol Cancer.* 2013;12(1):149.
- [8] Suo LG, Cui YY, Bai Y, et al. Anti-inflammatory TIPE2 inhibits angiogenic VEGF in retinal pigment epithelium. *Mol Immunol.* 2016;73:46–52.
- [9] Li D, Song L, Fan Y, et al. Down-regulation of TIPE2 mRNA expression in peripheral blood mononuclear cells from patients with systemic lupus erythematosus. *Clin Immunol.* 2009;133(3):422–427.
- [10] Gus-Brautbar Y, Johnson D, Zhang L, et al. The anti-inflammatory TIPE2 is an inhibitor of the oncogenic Ras. *Mol Cell.* 2012;45(5):610–618.
- [11] Fayngerts SA, Wang Z, Zamani A, et al. Direction of leukocyte polarization and migration by the phosphoinositide-transfer protein TIPE2. *Nat Immunol.* 2017;18(12):1353–1360.
- [12] Li Z, Guo C, Liu X, et al. TIPE2 suppresses angiogenesis and non-small cell lung cancer (NSCLC) invasiveness via inhibiting Rac1 activation and VEGF expression. *Oncotarget.* 2016;7(38):62224–62239.
- [13] Boissier P, Huynh-Do U. The guanine nucleotide exchange factor Tiam1: a Janus-faced molecule in cellular signaling. *Cell Signal.* 2014;26(3):483–491.
- [14] Wang Z, Fayngerts S, Wang P, et al. TIPE2 protein serves as a negative regulator of phagocytosis and oxidative burst during infection. *Proc Natl Acad Sci U S A.* 2012;109(38):15413–15418.
- [15] Zoncu R, Efeyan A, Sabatini DM. mTOR: from growth signal integration to cancer, diabetes and ageing. *Nat Rev Mol Cell Biol.* 2011;12(1):21–35.
- [16] Saxton RA, Sabatini DM. mTOR signaling in growth, metabolism, and disease. *Cell.* 2017;168(6):960–976.
- [17] Sancak Y, Bar-Peled L, Zoncu R, et al. Ragulator-Rag complex targets mTORC1 to the lysosomal surface and is necessary for its activation by amino acids. *Cell.* 2010;141(2):290–303.
- [18] Sancak Y, Peterson TR, Shaul YD, et al. The Rag GTPases bind raptor and mediate amino acid signaling to mTORC1. *Science (New York, NY).* 2008;320(5882):1496–1501.
- [19] Bar-Peled L, Schweitzer LD, Zoncu R, et al. Ragulator is a GEF for the rag GTPases that signal amino acid levels to mTORC1. *Cell.* 2012;150(6):1196–1208.
- [20] Zheng X, Liang Y, He Q, et al. Current models of mammalian target of rapamycin complex 1 (mTORC1) activation by growth factors and amino acids. *Int J Mol Sci.* 2014;15(11):20753–20769.
- [21] Yang H, Jiang X, Li B, et al. Mechanisms of mTORC1 activation by RHEB and inhibition by PRAS40. *Nature.* 2017;552(7685):368–373.
- [22] Saki A, Cantley LC, Carpenter CL. Rac1 regulates the activity of mTORC1 and mTORC2 and controls cellular size. *Mol Cell.* 2011;42(1):50–61.
- [23] Klionsky DJ. Autophagy: from phenomenology to molecular understanding in less than a decade. *Nat Rev Mol Cell Biol.* 2007;8(11):931–937.
- [24] Mizushima N. Autophagy: process and function. *Genes Dev.* 2007;21(22):2861–2873.
- [25] Klionsky DJ, Emr SD. Autophagy as a regulated pathway of cellular degradation. *Science (New York, NY).* 2000;290(5497):1717–1721.
- [26] Mehrpour M, Esclatine A, Beau I, et al. Autophagy in health and disease. Regulation and significance of autophagy: an overview. *Am J Physiol Cell Physiol.* 2010;298(4):C776–85.
- [27] Levine B, Klionsky DJ. Development by self-digestion: molecular mechanisms and biological functions of autophagy. *Dev Cell.* 2004;6(4):463–477.
- [28] Mizushima N, Levine B, Cuervo AM, et al. Autophagy fights disease through cellular self-digestion. *Nature.* 2008;451(7182):1069–1075.
- [29] Levine B, Kroemer G. Autophagy in the pathogenesis of disease. *Cell.* 2008;132(1):27–42.
- [30] Zhang J, Zhou W, Lin J, et al. Autophagic lysosomal reformation depends on mTOR reactivation in H2O2-induced autophagy. *Int J Biochem Cell Biol.* 2016;70:76–81.
- [31] Yu L, McPhee CK, Zheng L, et al. Termination of autophagy and reformation of lysosomes regulated by mTOR. *Nature.* 2010;465(7300):942–946.
- [32] Rong Y, McPhee CK, Deng S, et al. Spinster is required for autophagic lysosome reformation and mTOR reactivation following starvation. *Proc Natl Acad Sci U S A.* 2011;108(19):7826–7831.
- [33] Bjorkoy G, Lamark T, Brech A, et al. p62/SQSTM1 forms protein aggregates degraded by autophagy and has a protective effect on huntingtin-induced cell death. *J Cell Biol.* 2005;171(4):603–614.
- [34] Mizushima N, Yoshimori T. How to interpret LC3 immunoblotting. *Autophagy.* 2007;3(6):542–545.
- [35] Ichimura Y, Kumanomidou T, Sou YS, et al. Structural basis for sorting mechanism of p62 in selective autophagy. *J Biol Chem.* 2008;283(33):22847–22857.
- [36] Kimura S, Noda T, Yoshimori T. Dissection of the autophagosome maturation process by a novel reporter protein, tandem fluorescently-tagged LC3. *Autophagy.* 2007;3(5):452–460.
- [37] Mu Y, Yan X, Li D, et al. NUPR1 maintains autolysosomal efflux by activating SNAP25 transcription in cancer cells. *Autophagy.* 2018;14(4):654–670.
- [38] Klionsky DJ, Abdelmohsen K, Abe A, et al. Guidelines for the use and interpretation of assays for monitoring autophagy (3rd edition). *Autophagy.* 2016;12(1):1–222.
- [39] Ma C, Zhu L, Wang J, et al. Anti-inflammatory effects of water extract of *Taraxacum mongolicum* hand.-Mazz on lipopolysaccharide-induced inflammation in acute lung injury by suppressing PI3K/Akt/mTOR signaling pathway. *J Ethnopharmacol.* 2015;168:349–355.
- [40] Karonitsch T, Kandasamy RK, Kartnig F, et al. mTOR senses environmental cues to shape the fibroblast-like synovioocyte response to inflammation. *Cell Rep.* 2018;23(7):2157–2167.
- [41] Puertollano R. mTOR and lysosome regulation. *F1000Prime Rep.* 2014;6:52.

- [42] Perera RM, Zoncu R. The Lysosome as a Regulatory Hub. *Annu Rev Cell Dev Biol.* 2016;32(1):223–253.
- [43] Cherfils J. Encoding Allosterity in mTOR Signaling: the Structure of the Rag GTPase/Ragulator Complex. *Mol Cell.* 2017;68(5):823–824.
- [44] Dikic I, Elazar Z. Mechanism and medical implications of mammalian autophagy. *Nat Rev Mol Cell Biol.* 2018;19(6):349–364.
- [45] Perl A. mTOR activation is a biomarker and a central pathway to autoimmune disorders, cancer, obesity, and aging. *Ann N Y Acad Sci.* 2015;1346(1):33–44.
- [46] Rong Y, Liu M, Ma L, et al. Clathrin and phosphatidylinositol-4,5-bisphosphate regulate autophagic lysosome reformation. *Nat Cell Biol.* 2012;14(9):924–934.
- [47] Liu X, Klionsky DJ. Regulation of autophagic lysosome reformation by kinesin 1, clathrin and phosphatidylinositol-4,5-bisphosphate. *Autophagy.* 2018;14(1):1–2.
- [48] Fayngerts SA, Wu J, Oxley CL, et al. TIPE3 is the transfer protein of lipid second messengers that promote cancer. *Cancer Cell.* 2014;26(4):465–478.
- [49] Schaaf G, Ortlund EA, Tyeryar KR, et al. Functional anatomy of phospholipid binding and regulation of phosphoinositide homeostasis by proteins of the sec14 superfamily. *Mol Cell.* 2008;29(2):191–206.
- [50] Li Y, Zhao M, Guo C, et al. Intracellular mature IL-37 suppresses tumor metastasis via inhibiting Rac1 activation. *Oncogene.* 2018;37(8):1095–1106.
- [51] Woods GL, Walker DH. Detection of infection or infectious agents by use of cytologic and histologic stains. *Clin Microbiol Rev.* 1996;9(3):382–404.
- [52] Deng Q, Pan B, Alam HB, et al. Citrullinated histone H3 as a therapeutic target for endotoxic shock in mice. *Front Immunol.* 2019;10:2957.